Journal of Ceramic Processing Research. Vol. 21, No. 3, pp. 331~337 (2020)
(Received 12 December 2019, Received in revised form 20 March 2020, Accepted 24 March 2020)
https://doi.org/10.36410/jcpr.2020.21.3.331

J O U R N A L O F
Ceramic Processing Research

An automated longquan celadon glaze thickness measurement method based on optical coherence tomography

Yang Zhou*, Longjie Shi, Gang Ceng, Tiebing Liu, Yang Shi, Zhengwei Chen, Fenglin Wang and Yuefeng Ceng
School of Information and Electronic Engineering, Zhejiang University of Science and Technology, Hangzhou 310023, PR China

The thickness of glaze is one of the important indicators in the quality evaluation of Longquan celadon. But till now, there is no automatic and non-destructive method to measure it. In order to satisfy this demand, an automated method has been proposed to measure the glaze thickness based on optical coherence tomography (OCT) technique. According to the morphological characteristics of celadon glaze in OCT image, the proposed method locates the upper and lower boundaries of the glaze layer, then the glaze thickness is automatically calculated after the axial resolution calibration of the OCT images for different categories of Longquan celadon. In the experiment, the glaze OCT images of 6 different categories of Longquan celadon were applied in the glaze thickness estimation. By comparing with the physical measuring result, this method is proved to be able to measure the glaze thickness rapidly and non-destructively and the performance is enough to meet the demand of the industrial application.

Key words: Optical coherence tomography (OCT), Longquan celadon, Glaze, Thickness.

Introduction

Longquan celadon is the only Chinese ceramics listed to the world's intangible heritage, and its craftsmanship is a representative among Chinese ceramics [1]. However, affected by composition of the ceramic body, temperature, glaze and other factors during the firing process, the proportion of superior grade products of Longquan celadon is relatively small, which hinders the further development of the Longquan Celadon industry [2]. Therefore, the non-destructive inspection of the finished celadon products, especially the craftsmanship evaluation, is vital to the promotion of Longquan celadon development.

The main phases in the ceramic body of the Longquan celadon products are quartz (SO_2), mullite, few glass phases and pores, while the glaze consists of bubbles, glass phases and crystals. For superior celadon products, there is no obvious boundary between the glaze and the ceramic body, and the homogeneity of glaze layer is good [3, 4]. During the manufacture procedure, the factors that affect the quality of glaze are complicated, including the characteristics of the ceramic body and glaze themselves (body-glaze expansion coefficient, glaze tensile strength, elastic modulus and etc.), tackiness of the body and glaze (middle layer formation condition), thickness of glaze, cooling rate, and etc. The thickness of glaze is a significant indicator to evaluate the quality of the ceramics. For example, the glaze color saturation is stronger when the glaze is thicker [5]. And the glaze thickness is also closely related to the glaze stress. The precise control of the glaze thickness can keep the glaze stress balance between tensile stress and comprehensive stress, which is critical to prevent the glaze cracking.[6] Because the Longquan celadon products has high yield and the glaze thickness of the individual products differs from each other, even from the same batch, the destructive (physical) measurement of the celadon glaze layer thickness does not meet the needs of the industrialization development. However, there is still no related reports on the nondestructive measurement methods so far.

Optical coherence tomography (OCT), which is an optical image technique based on confocal microscope and Michelson interference theory, has the advantages of high resolution and nondestructive examination [7]. At present, the OCT imaging technique has been successfully applied to ophthalmology [8-10], material analysis [11], archaeology [12], thickness measurement of organizations and other fields [13]. In the meantime, OCT imaging technique has also provided a new method for the nondestructive analysis for structure of ceramics glaze [14]. Yang M et al. analyzed the size and distribution of the bubbles in the Song dynasty ceramics glaze by OCT technique and had proved that the radios of calcite and alumina in the glaze can affect the texture and color of ceramics [15]. Yan X et al. have provided a discrimination method of the ceramics

*Corresponding author:
Tel : +86 13868077650
Fax: +86 57185070300
E-mail: zybuaa@163.com

glaze origin and kiln based on feature difference in glaze OCT image [16, 17]. Zhong et al. have classified the glaze layer according to OCT image texture feature combined with PCA method [18]. Those research achievements above have indicated the OCT imaging technique can be possibly applied to the glaze layer planar reconstruction and observation of the subsurface structure of Longquan celadon and be further used for the measurement of the glaze thickness with the advantage of fast and easy operation.

The possibility of revealing the internal structure characteristics of Longquan celadon glaze and measuring the glaze thickness non-destructively via OCT imaging technique has been studied. Also, it has put forward an automated method to measure the glaze thickness through OCT imaging technique realized by the automatic location of the upper and lower boundaries of the glaze and calculation of the pixel distance between in the OCT image.

Materials and Methods

Celadon sample collection and image capture

Typical samples of Longquan celadon from Ge Kiln and Di Kiln were collected. The sample from Ge Kiln was purchased in Longquan Lingqing Ceramics Workshop and those from Di Kiln was purchased in Longquan Kongshanxinyu Ceramics, both of which are local celadon manufacturing enterprises. Both of the two categories of samples were teacups with lavender gray glaze, plum green glaze and ivory glaze. All the OCT images were captured by the OQ Labscope system manufactured by Lumedica and the scan area of celadon glaze surface was randomly selected. The central wavelength, sensitivity, linear scanning scope, axial resolution, lateral resolutions, imaging depth in the air and image resolution of the system were 840 nm, 100 dB, 0-7 mm, 7 μm, 15 μm, 3.6 mm, 512*512 pixel, respectively. During the image capture, there was no need to do the pretreatment and the Fig. 1 below shows the OCT images of 6 different categories of Longquan celadon glaze.

Boundaries extraction and glaze thickness calculation

Through monitoring the ballistic and snaking photons of the samples reflected from the scattering medium in samples and interfering with the reference light, the OCT technique showed the luminance changes caused by different phases in the glaze as the change of the refractive index. Fig. 2 below is a typical cross-section view and its corresponding OCT image of Longquan celadon glaze, and the area with higher grayscale value (ash gray) in the OCT image was named scattering phase.

In the image capture procedure, the back scattering light was intensified on the glaze upper boundary because of the refractive index change on the boundary between the air and celadon glaze, therefore there was an obvious bright scattering phase in the OCT image. The refractive indexes of the crystal particles and bubbles were different, the light intensity on the bubbles and crystal particles looked different in glaze layer where large quantities of bubbles exited. In the OCT

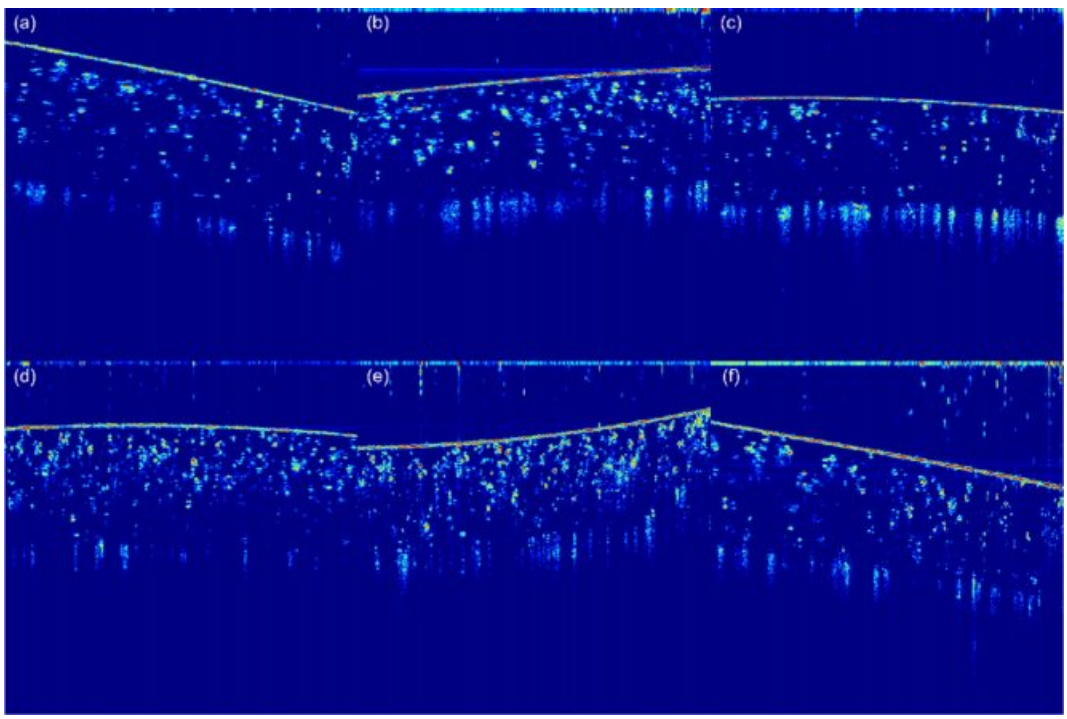

Fig. 1. OCT images of 6 different categories of Longquan celadon teacup glaze. (a) Di Kiln lavender grey glaze; (b) Di Kiln plum green glaze; (c) Di Kiln ivory glaze; (d) Ge Kiln lavender grey glaze; (e) Ge Kiln plum green glaze; (f) Ge Kiln ivory glaze.

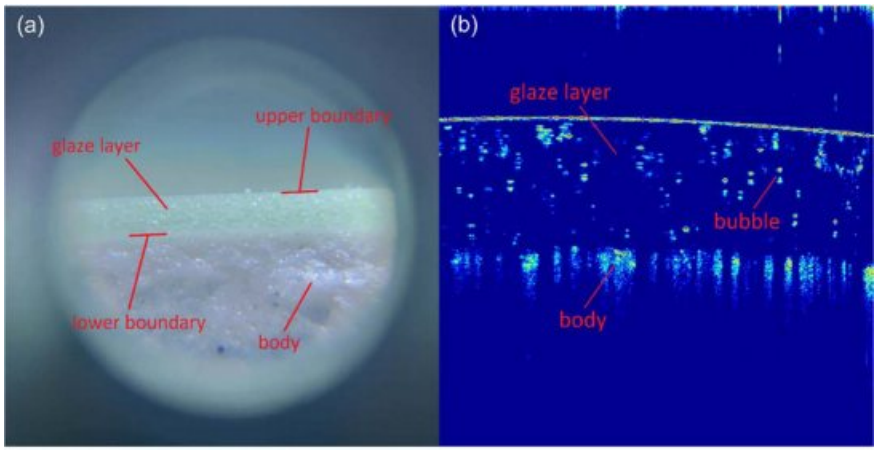

Fig. 2. Typical Longquan celadon glaze. (a) Cross-Section view; (b) OCT image.

image, a bubble was showed as two bright short parallel scattering phases and the interior of the bubble was showed as blank space. Similarly, the crystal particles were showed as clusters of scattering phases with different sizes and contrasts. In addition, scattering light got weaker in deeper depth, which was the reason why the scattering phase close to the upper boundary was brighter than those far away from the upper boundary. During the firing operations, the melted glaze permeated into the body. As the refractive index of the glaze is different from that of the body, the scattering of the whole penetrating area (the interface between the glaze and the body) was strong, which was showed as bright ribbon stretch defined as strip scattering phase in the OCT image. In our study, we proposed the method to automated measure the glaze thickness by locating the upper and lower boundaries according to the morphological characteristics of celadon glaze layer in the OCT image (Showed in Fig. 3), and it was realized by a Matlab program (Mathworks, Massachusetts, USA).

Extraction of the glaze upper boundary

In the glaze OCT image, the scattering phases of upper boundary, which were located at the top of all scattering phases and stretched across the entire image were brighter than other phases. The following steps have been taken to locate the upper boundary.

Step 1: To reduce the sparkle and conjugate noise in the OCT image while locating the upper boundary of the glaze layer, median filtering with [3*5] window was used according to pixel grayscale similarity.

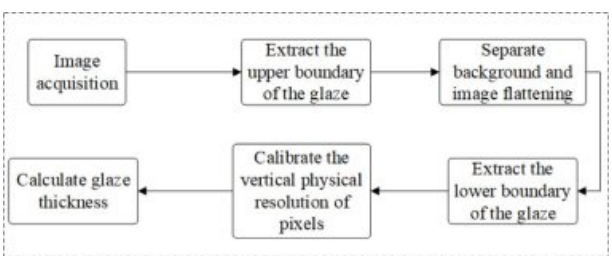

Fig. 3. Flow chat of the method to measure the Longquan celadon glaze thickness.

Step 2: To increase the grayscale difference between the glaze upper boundary and the background, OSTU was applied to determine the threshold of the image binarization and the flitted image was changed to binary image by canny operator [19]. The banalization reduced the image size and enhanced the pixel grayscale contrast at the junction of the glaze upper boundary and the air.

Step 3: The non-zero pixels belonging to the same 8 connected region in the binary image were gathered as one part of glaze. And in order to smooth the profile of the glaze upper boundary and decrease influence from non-glaze pixels, a disk structure element whose radius was 5 has been adopted to do the closed operation. As a result, the grayscale values out of the glaze were set to 0 (black).

Step 4: The top non-zero pixel of each column was extracted as one point of the upper boundary.

Step 5: The Lagrange interpolation polynomial was used to fit all the boundary points collected in the step 4. And the fitted boundary was regarded as the final upper boundary of the glaze.

Background separation and image flattening

The air, background part of the image, was polluted by speckle and conjugate noise. Based on the previous knowledge, clipping the background from the image can directly clear the noise and reduce the noise influence when locating the lower boundary. The grayscale of pixels above the glaze upper boundary in the OCT image were set to zero as the background was separated. Because the fitted glaze upper boundary was a smooth curve, in order to reduce the error from the curvature when locating the lower boundary and measuring the thickness, the highest point in the upper boundary was used as a standard and every column was upward to make every boundary point at the same

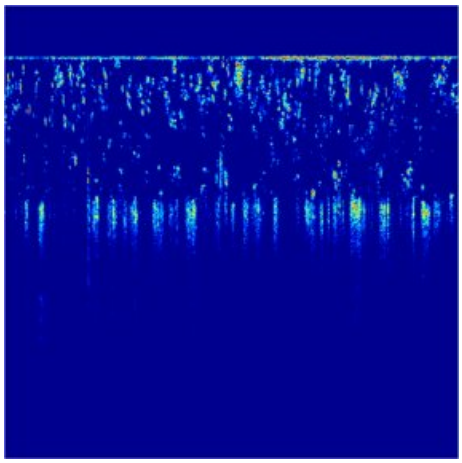

Fig. 4. Background separation and image flattening.

horizontal. And then the row coordinate of the glaze upper boundary was set as the location U for subsequent calculation. Fig. 4 shows the image after background separation and image flattening.

Extraction of the glaze lower boundary

According to the characteristics of glaze lower boundary in the OCT image, the morphological manipulation was chosen to locate the boundary. First, in order to highlight the grayscale difference between the scattering phases and background in the image, the CLAHE algorithm was adopted to strengthen the gray contrast of the flattened image [20]. As every scattering phase occupied a very small space in the glaze, there were short connections between them. Therefore the flat disk structure element whose radius was 5 pixel was used for opening operation to increase the contrast. As a result, the connections among the internal scattering phases in the glaze were disconnected. Secondly, in order to highlight the location of the ceramic body, the flattened image was regarded as the mask, then a continuous dilation operation was conducted as morphological image reconstruction after above opening operation so that the contrast of the ceramic body and glaze was strengthened [21]. After the steps above, there were holes left within the scattering phases of the ceramic body part in the OCT image. Therefore, dilation operation based on flat disk structure element whose radius was 3 pixel was used to refill the holes. Finally, the OTSU method was applied to binarize the image. The lower part of OCT image, shown as stripes, were regarded as the ceramic body, and the top of every stripe target were the boundary between body and glaze, defined as glaze lower boundary. Unfortunately, the stripe targets in the glaze part of OCT image were discontinuous, so the mean value of upper boundary location (ordinate) of the stripe targets was considered as the glaze lower boundary for the glaze thickness measurement. The whole procedure of the glaze lower boundary extraction is shown in Fig. 5.

Resolution calibration and glaze thickness measurement

In the flattened OCT image, the product of the pixel

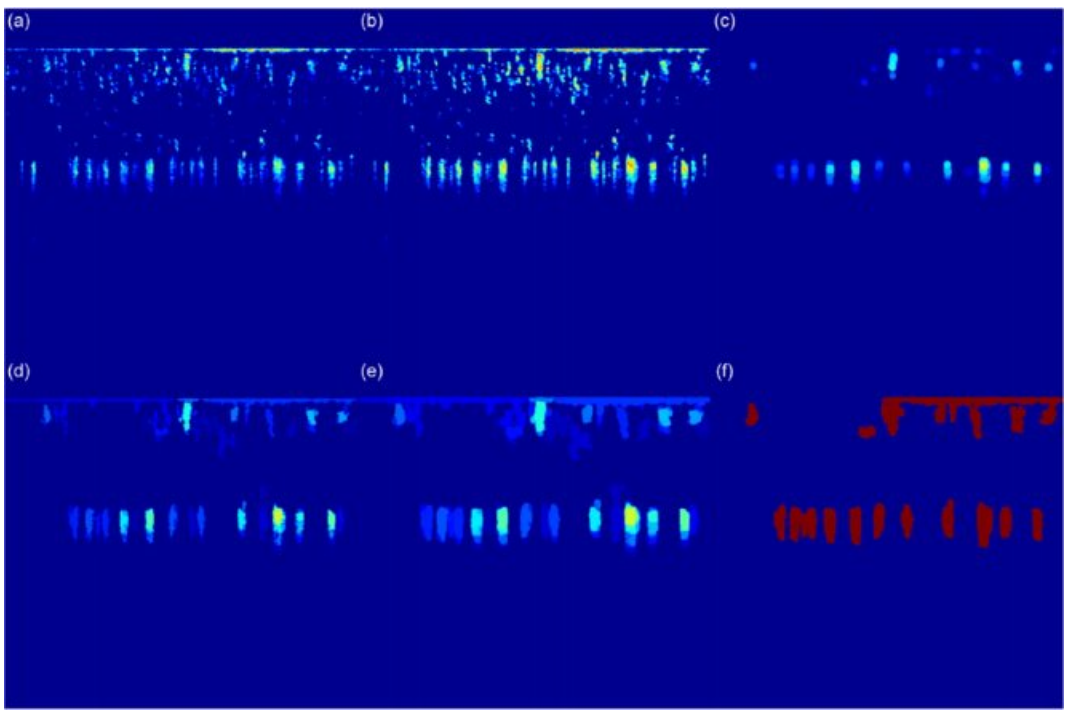

Fig. 5. Extraction of celadon glaze lower boundary. (a) Image flattening; (b) Image contrast strengthening; (c) Morphological opening; (d) Image reconstruction; (e) Image dilation; (f) Image binarization.

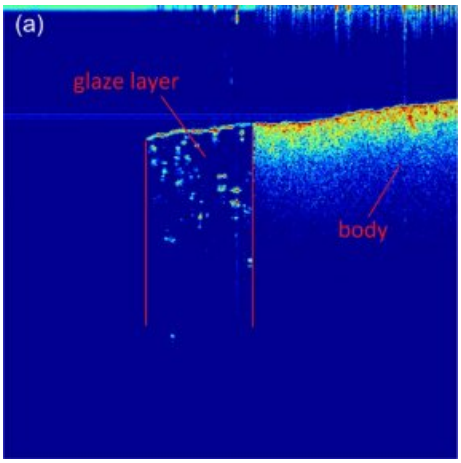

Fig. 6. Cross-sectional view of celadon glaze.

distance between the glaze upper and lower boundary and the axial resolution of the pixel in the glaze was the thickness of the glaze. As the refractive index of the air was different from that of the celadon glaze, the pixel axial resolution in the air calibrated by the OCT system manufacturer was not applicable to calculate the thickness. Therefore, the pixel axial resolution needed to be re-calibrated for different type of celadon glaze. The calibration process was followed: 1). Set the scanning parameters corresponding to the parameters when capturing the samples; 2). Choose the typical celadon fragments of every category sample and scan the cross-section of the fragments as presented in Fig. 6; 3). The lateral resolution of OCT system was the same in the air and the glaze, use the OCT self-equipped caliper to measure the celadon glaze thickness T_x (distance between the 2 red lines shown in Fig. 6; 4). For the same area, adjust the objective lens and vertical scan the glaze of test sample in accordance with the scan mode of Fig. 3, 4, 5 to get the glaze OCT image, then locate the upper and lower boundaries, and calculate the pixel distance D between the upper and lower boundaries ($D = B_{avg} - U$, where B_{avg} and U were respectively the mean coordinate of the glaze lower boundary pixel points and the coordinate of the upper boundary); 5).Calculate the pixel axial resolution (Pr_x) of the celadon glaze according to formula (1);

$$Pr_x = \frac{T_x}{D} \tag{1}$$

For an unknown glaze thickness sample of Longquan celadon, the glaze upper and lower boundaries were located, then the pixel distance D between the boundaries was calculated ($D = B_{avg} - U$), finally the glaze thickness was the product of the pixel distance D and the pixel axial resolution (Pr_x) in the glaze.

Results and Discussion

The glaze upper and lower boundaries of the typical experiment samples of lavender gray glaze, plum green glaze and ivory glaze respectively from Ge Kiln and Di Kiln are shown in Fig. 7. In Fig. 7, the glaze upper boundary had higher grayscale than that of the background in the OCT image and the fitted upper

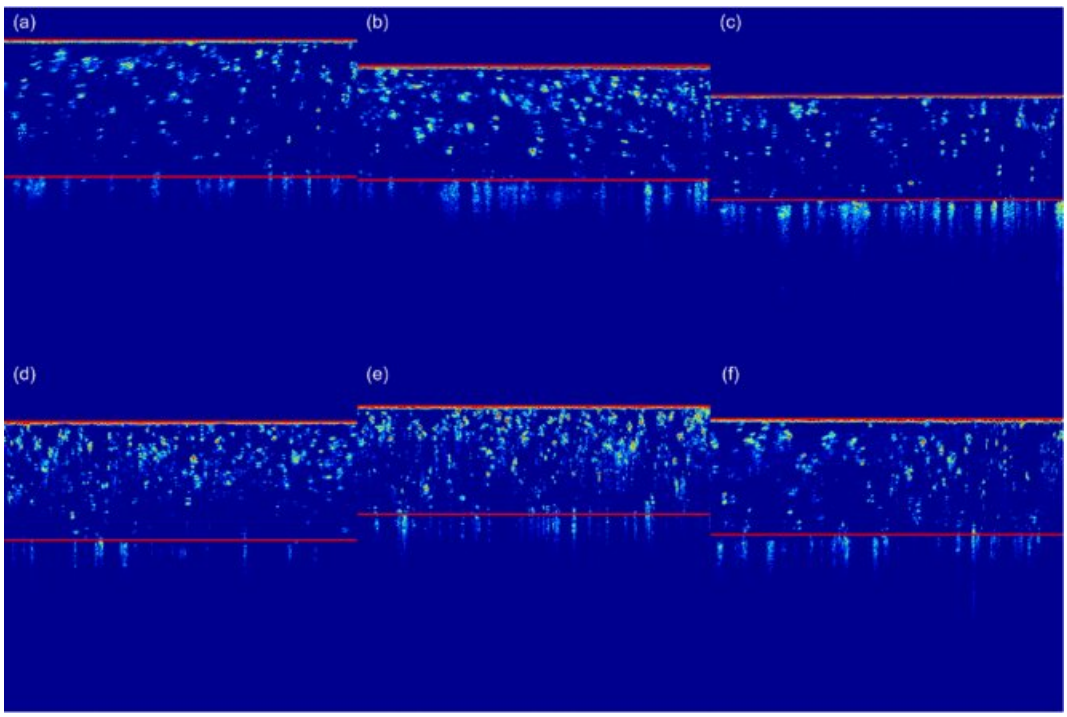

Fig. 7. Location of glaze upper and lower boundaries of the 6 categories of Longquan celadon. (a) Di Kiln lavender gray glaze; (b) Di Kiln plum green glaze; (c) Di Kiln ivory glaze; (d) Ge Kiln lavender gray glaze; (e) Ge Kiln plum green glaze; (f) Ge Kiln ivory glaze.

Table 1. Thickness measurement results of different categories of longquan celadon glaze.

Type	Ge kiln powder green glaze	Ge kiln plum green glaze	Ge kiln Ivory glaze	Di kiln powder green glaze	Di kiln plum green glaze	Di kiln Ivory glaze
D (Pixel Distance)	167	143	167	193	166	149
Pr_x/μm (Resolution)	3.35	3.74	3.38	3.03	3.22	3.34
Thickness	559.4	534.8	564.4	584.7	534.5	497.66
T_x/μm (Physical Examination)	540.0	520.0	560.0	580.0	540.0	500.0

boundary well overlapped the real boundary which proved that the proposed method can accurately locate the glaze upper boundary. When flattening the glaze layer, taking the top point of the glaze upper boundary for reference avoided the error while measuring the glaze thickness caused by the curve profile. In addition, in the OCT images of all types of celadon glaze, the scattering phases of the ceramic body were discontinuous, which made it more difficult to locate the lower boundary of the glaze layer. But from Fig. 7, it still can be seen that the proposed method detected the lower boundary which was interfered by the bubbles and with seriously weakened surface scattered light. Totally 60 samples of the 6 categories (10 for each category) have been tested, and the result showed that the upper and lower boundaries of the glaze can be used for further accurate measurement of the glaze thickness.

After calibrating the axial resolution, the glaze thickness of 6 different categories of typical Longquan celadon teacup samples have been measured. And in the meantime, the teacups have been destructively cut and the glaze thickness has been measured artificially. For reference, the comparison result is showed in Table 1. While calibrating the resolution, accuracy of both OCT system and proposed method were at micrometer level, which was suitable for industrial application. Compared with the physical destruction method, the absolute error was less than 50 micrometer and the relative error was less than 5%, which has verified the proposed method can be adopted for the rapid and nondestructive measurement of the glaze thickness.

The glaze thickness of Longquan celadon is closely related to its quality. On the one hand, the thickness of the celadon glaze affects the color generation of the glaze, on the other hand, it also affects the glaze stress between the ceramic body and the glaze [22]. The precise control of the glaze thickness can effectively prevent the glaze from cracking and improve the celadon quality. Overall, the glaze thickness of high-quality celadon is almost uniform, more, by examining the uniformity of the celadon glaze thickness, the quality of celadon can be judged.

The OCT imaging technique can present the internal organization structure of the celadon glaze non-destructively at micrometer resolution level. Before our study, the OCT imaging technique has already been applied to the identification and classification of the different categories of ceramics by discriminating the internal structure characteristics of the glaze [23-26]. But on the measurement of the celadon glaze thickness, there are few literature reports. In this study, the thickness of the celadon glaze has been accurately measured, which has expanded the application of OCT imaging technique to the celadon quality detection.

Conclusion

In this study, an automated method for the Longquan celadon glaze thickness measurement based on OCT technique has been put forward. The upper boundary of the glaze was located by the characteristics of its scattering phases and optimized by the Lagrange polynomial interpolation. Then the image was treated by background separation and image flattening, and the glaze lower boundary was located by the morphological manipulation. After the calibration of the glaze axial resolution in the OCT image, the rapid and non-destructive measurement of glaze thickness was finished by calculation of the distance between the upper and lower boundaries. The method proposed in this study fills the blank of automated evaluation method for glaze thickness of the Longquan celadon product, one of important quality indicators, and speeds up the industrialization of the Longquan celadon.

In the experiment of this study, the approach was essentially based on tomography of the glaze layer but not the three-dimensional data. The glaze thickness will be more widely and accurately measured if the algorithm utilizes the three-dimensional structure from OCT technique. That is what we are planning to do in the future study.

Acknowledgments

This work was supported by National Key R&D Program of China (No. 2018YFF0213400), the Inter-disciplinarily Pre-research Project of Zhejiang University of Science and Technology (No. 2013JC07Y), and Public Basic Research Program of Zhejiang Province (No. LGN19B050002).

References

1. X. Zhang, J. Zhang, Ceram. Stud. 33 (2018) 110-113.
2. Q. Shi and D.A. Hassan, JOM. 71 (2018) 1016-1023.
3. Q. Shi, J. Synth, Cryst. 46 (2017) 2527-2532.

4. H.B. Zghal, M. Medhioub, and T. Mhiri, J. Ceram. Process. Res. 13 (2012) 202-2091.
5. Q. Chen, Y. Zhou, and S. Zhou, J. Ceram. 47 (1996) 42-47.
6. Y. Gao and Q. Geng, Ceram. 5 (2003) 24-26.
7. D. Huang, E.A. Swanson, C.P. Lin, J.S. Schuman, W.G. Stinson, W. Chang, M.R. Hee, T. Flotte, K. Gregory, C.A. Puliafito, and J.G. Fujimoto, Sci. 254 (1991) 1178-1181.
8. O. Müller, M.G. Todorova, T. Schlote, and K. Mon, Augenh. 235 (2018) 436-444.
9. Y. Li, Y. Zhang, S. Chen, Vernon G, W.T. Wong, and H. Qian, Invest. Ophthalmol. Vis. Sci. 59 (2018) 1084-1094.
10. S. Philipp, W. Sebastian, K. Sophie, B. Hrvoje, S. Thomas, G. Bianca, D. Rene, S.E. Ursula, and L. Georg, IEEE Trans. Med. Imaging. 38 (2019) 1037-1047.
11. Y. Zhou, Y. Zhao, S. Kim, and A. Wax, Opt. Mater. Express. 8 (2018) 622-628.
12. S. Yang, R. Zhu, L. Mi, Y. Cao, and Q. Li, Acta Optica Sinica. 35 (2015) 147-152.
13. L.M. Heindl, W. Adler, and O. El-Malahi, J. Glaucoma. 27 (2018) 1086-1093.
14. J. Li, B. He, W. Liu, X. Yan, S. Li, and Q. Li, Spectrosc. Spect. Anal. 36 (2016) 1500-1507.
15. M. Yang, A.M. Winkler, J. Klein, and J.K. Bartong, Stud. Conserv. 57 (2012) 67-75.
16. X. Yan, J. Dong, Q. Li, G. Musen, and Y. Hu, CHIN. J. Lasers. 41 (2014) 195-200.
17. Xin Y, J.Q. Dong, Q.H. Li, M.S. Guo, and Y.Q. Hu, Spectrosc. Spect. Anal. 35 (2015) 2275-2280.
18. D.X. Zhong, M.S. Guo, Y.Q. Hu, S. Liu, J.Q. Dong, and Q.H. Li, CHIN. J. Lasers. 45 (2018) 140-151.
19. N. Otsu, IEEE Trans. Syst. Man. Cybern. SMC-9 (1979) 62-66.
20. N.M. Sasi and V.K. Jayasree, Eng. 5 (2013) 326-331.
21. L. Vincent, IEEE Trans. Image Process. 2 (1993) 176-201.
22. X.H. Xu, Z.G. Wang, J.F. Wu, G.H. Leng, and D.K. Deng, J. Wuhan. Univ. Technol. 31 (2009) 55-58.
23. A.G. Turk, M. Sabuncu, and M. Ulusoy, Braz. Oral. Res. 32 (2018) e5.
24. W. Li, J. Liu, and Z. Zhang, J. Biomed. Opt. 23 (2018) 1-5.
25. C. Lin, W. Kuo, Y. Chang, J. Yu, and Y. Lin, Dent. Mater. 30 (2014) 910-916.
26. R. Su, M. Kirillin, P. Ekberg, A. Roos, E. Sergeeva, and L. Mattsson, Opt. Express. 20 (2012) 4603-4618.